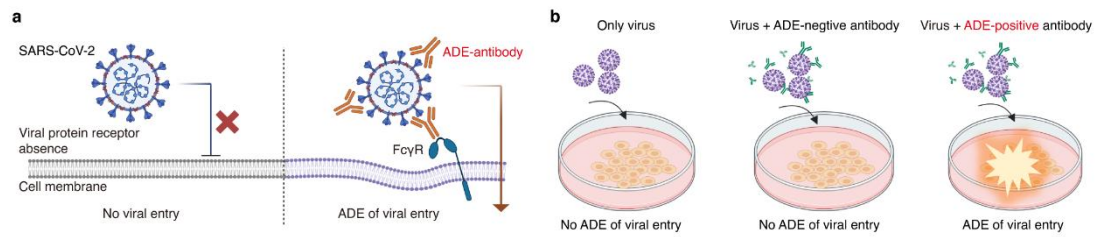


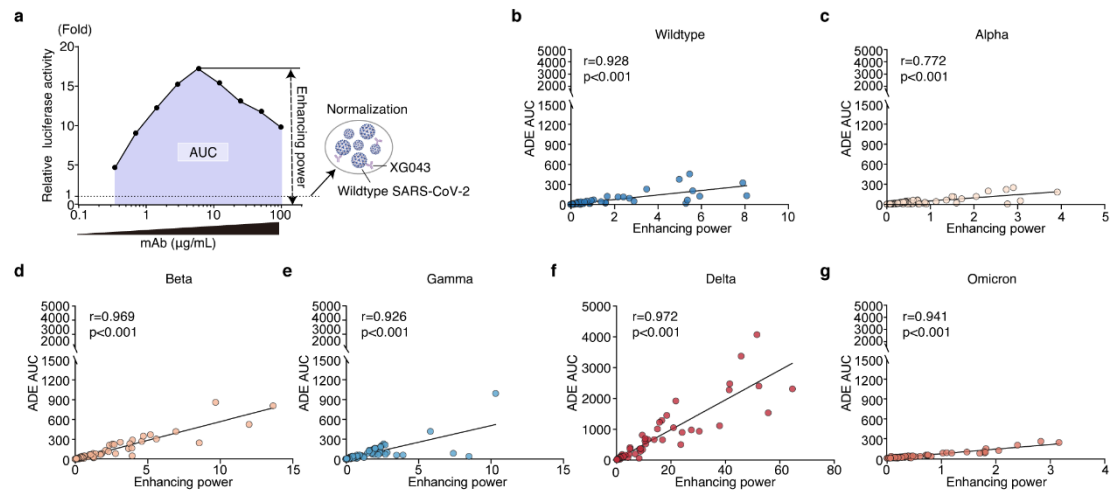
Supplementary Information



Supplementary Fig. S1: Mechanisms of ADE of viral entry.

(a) Schematic of ADE of viral entry mediated by FcγRs. Antibody Fab fragments bind SARS-CoV-2 S proteins while Fc regions engage FcγRs on immune cells, facilitating viral entry.

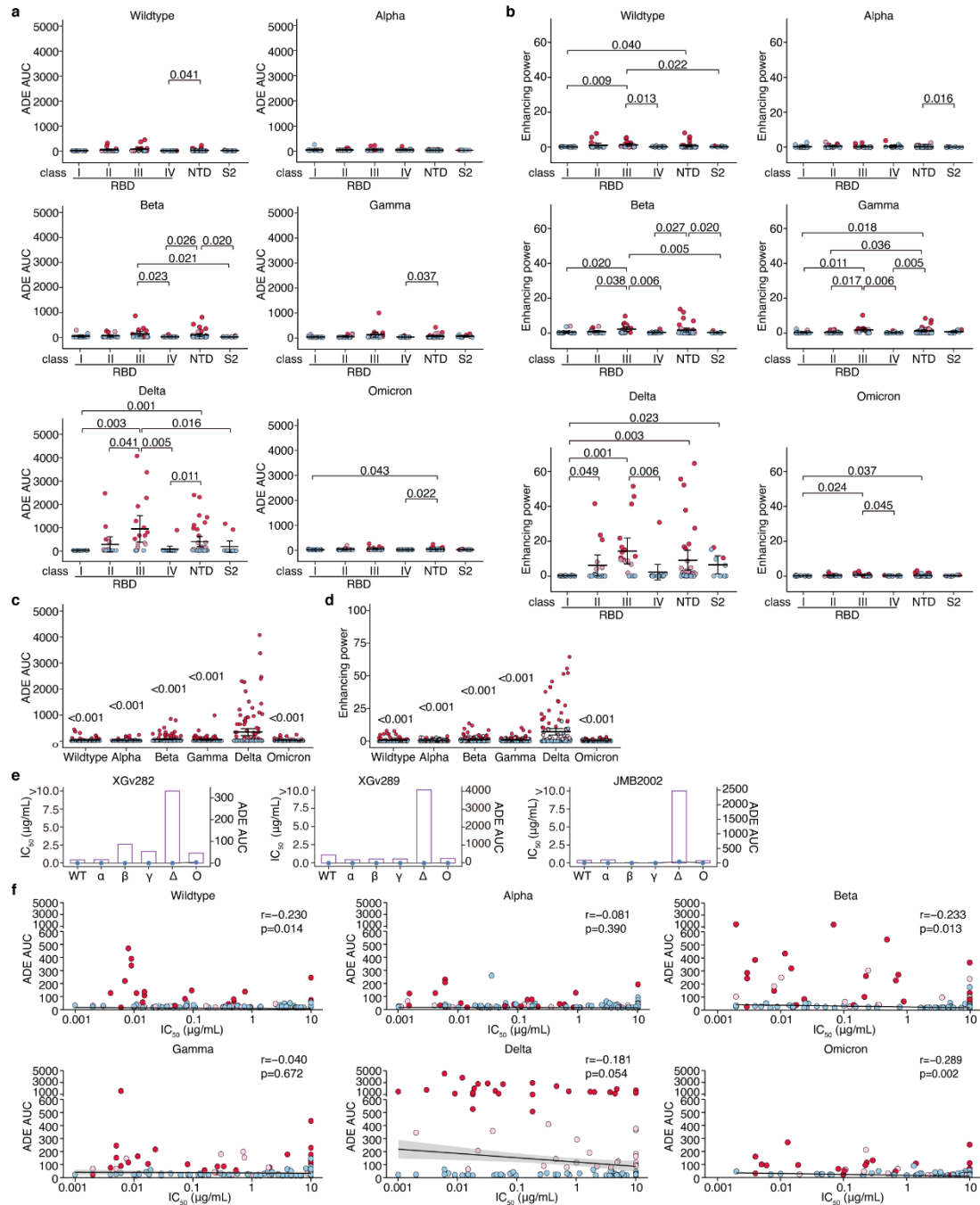
(b) In vitro pseudovirus ADE assay design. Raji cells expressing FcγRIIB (lacking host receptor ACE2) serve as target cells. S-expressing pseudoviruses encoding luciferase reporter require ADE-positive antibodies for FcγR-mediated entry and subsequent luciferase expression. Viral entry is quantified by measuring luciferase activity.



Supplementary Fig. S2: Quantitative metrics for ADE activity.

(a) Schematic illustrating two ADE quantification parameters. ADE area under curve (ADE AUC) integrates concentration-dependent enhancement, while ADE enhancing power represents maximum viral entry efficiency across antibody dilutions.

(b-g) Correlation between ADE AUC and enhancing power for all mAbs against SARS-CoV-2 variants, including wildtype **(b)**, Alpha **(c)**, Beta **(d)**, Gamma **(e)**, Delta **(f)**, and Omicron **(g)**. Each dot represents individual mAbs ($n = 114$). Solid lines show linear regression fits, with statistics calculated using Spearman's rank correlation method.



Supplementary Fig. S3. Enhanced ADE in Delta variant associated with S epitopes rather than neutralizing efficiency.

(a-b) Comparative ADE AUC (a) and enhancing power (b) of mAbs grouped by S epitope specificity across SARS-CoV-2 variants. Each dot represents a mAb. Data show mean \pm SD of at least two technical replicates.

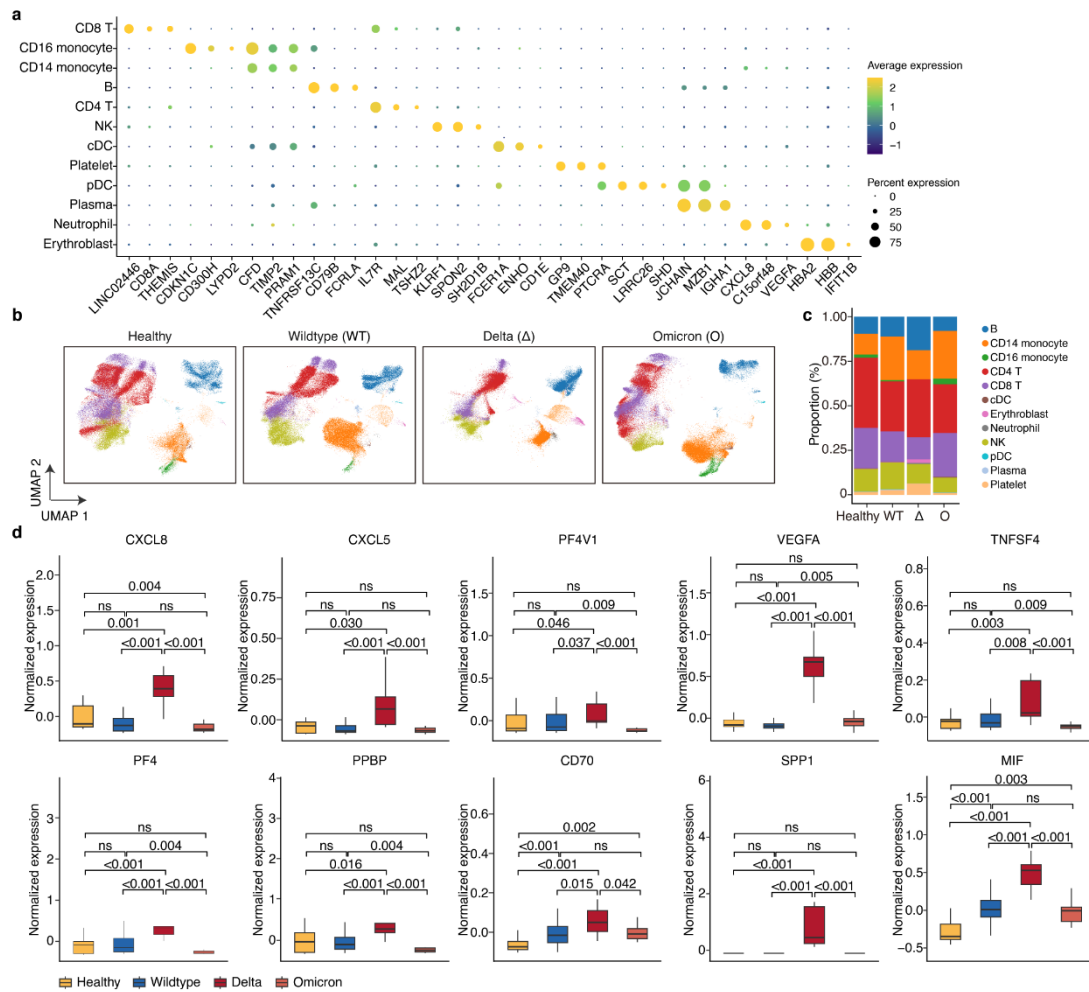
(c-d) ADE AUC (c) and enhancing power (d) for wildtype and VOCs relative to Delta. Each dot represents a mAb. Data show mean \pm SD.

(e) ADE AUC (bar) and IC_{50} (dot and line) values across VOCs for mAbs XGv282, XGv289, and JMB2002.

(f) Correlation analyses of ADE AUC versus IC_{50} values for all mAbs across SARS-CoV-2 variants. Each dot represents an individual mAbs ($n = 114$). Solid lines show linear regression fits. Statistics

calculated using Spearman's rank correlation method.

(a-d) Statistical analyses assessed using Kruskal-Wallis test with Dunnett's multiple comparisons and corrected with Benjamini-Hochberg adjustment.



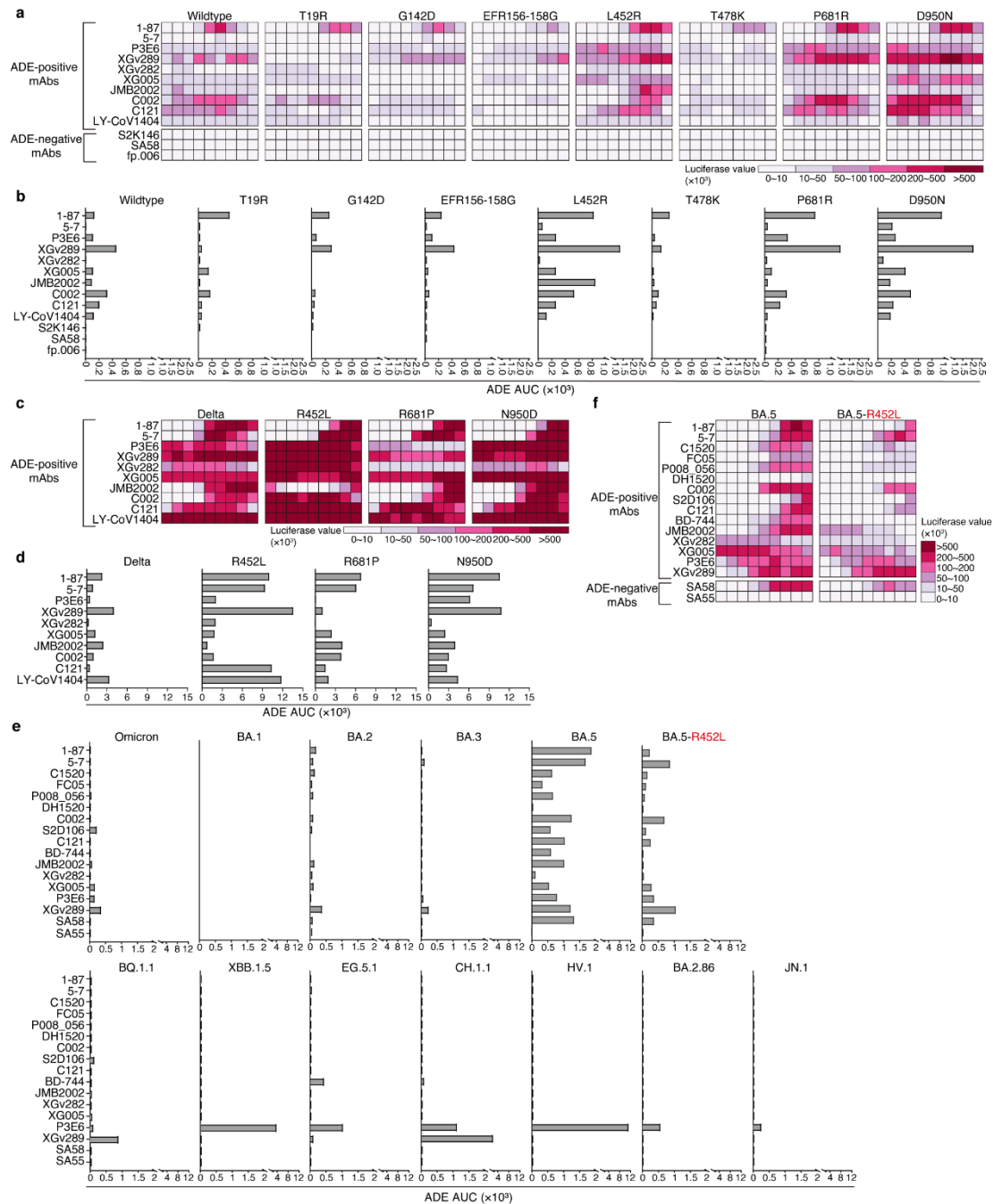
Supplementary Fig. S4: Integrated scRNA-seq analysis of PBMCs from SARS-CoV-2-infected patients and healthy controls.

(a) Expression distribution of canonical markers defining major PBMC populations (rows) across key genes (columns).

(b) UMAP projection of single PBMCs from healthy controls (n = 14) and patients infected with wildtype SARS-CoV-2 (n = 48), Delta (n = 9), or Omicron (n = 19). Each dot represents a single cell colored by annotated cell types.

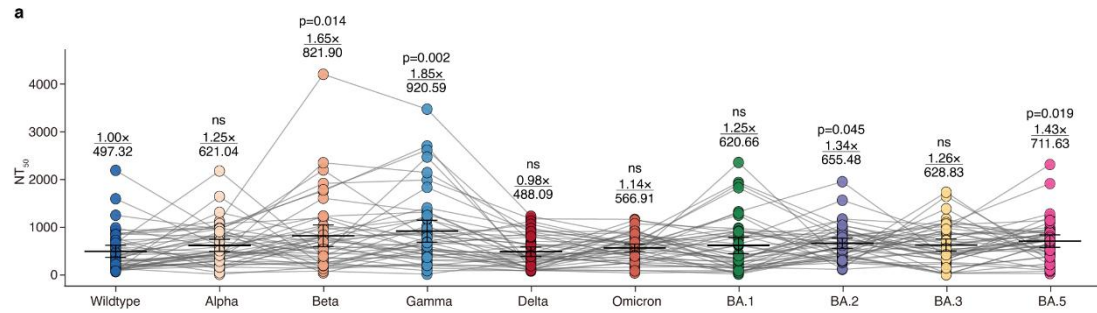
(c) Compositional analysis of immune cell subsets across cohorts. Stacked bars show average proportions.

(d) Cytokine gene expression across cohorts. Box plots show the median (center line), interquartile range (box limits), and minimum and maximum range (whiskers). Statistical analyses calculated using Kruskal-Wallis test with Dunnett's multiple comparisons and corrected with Benjamini-Hochberg adjustment.



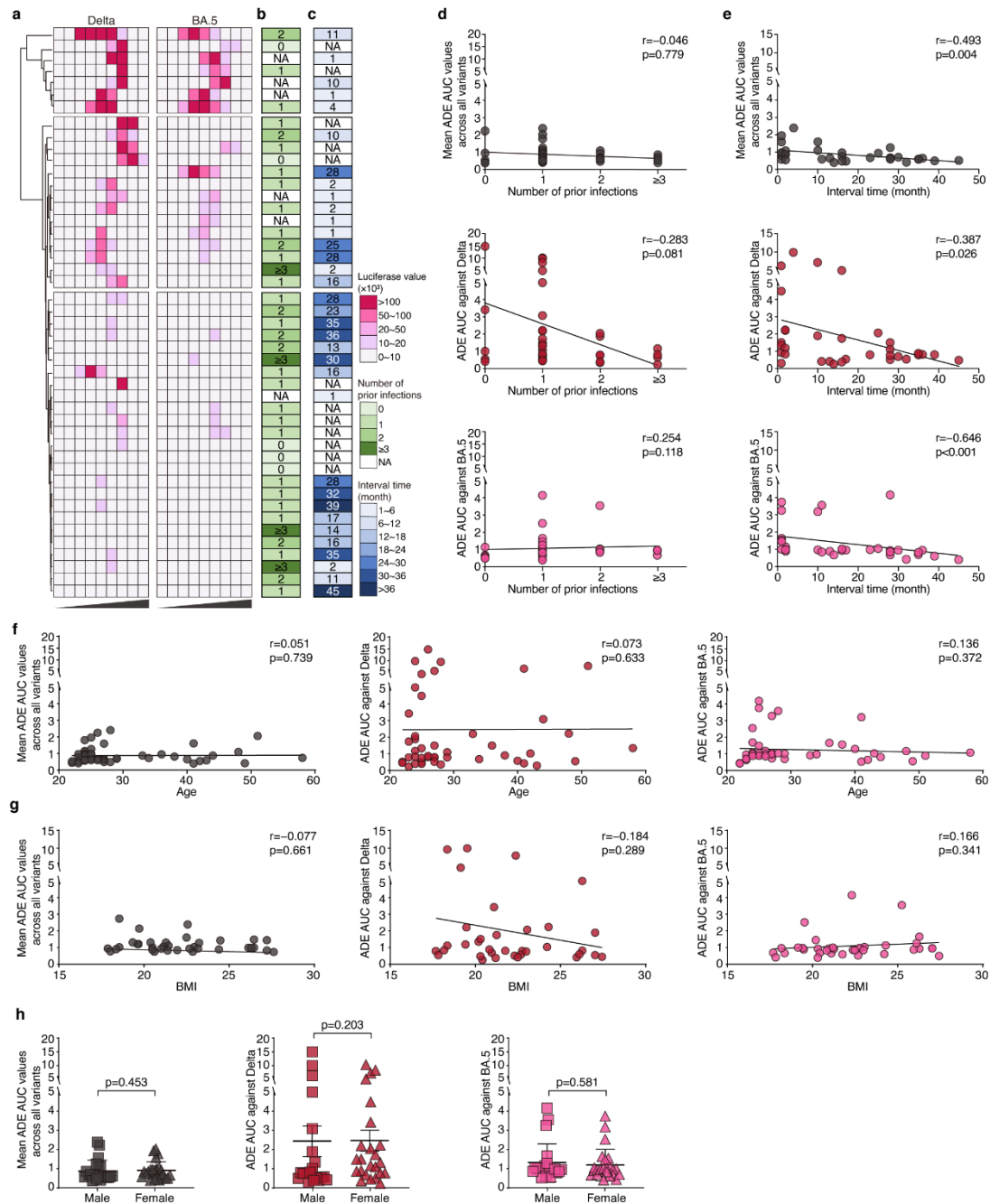
Supplementary Fig. S5: ADE activity against across diverse S mutants.

(a, c and f) Heatmap depicting in vitro ADE activity against the wildtype SARS-CoV-2 and its related point-mutant pseudoviruses (a), the Delta variant and its related point-mutant pseudoviruses (c), and the BA.5 and BA.5-R452L mutant pseudoviruses (f). Each mAb (rows) was tested at nine-point three-fold dilutions (columns) starting from 100 $\mu\text{g/mL}$. Relative luminescence intensity reflects viral entry efficiency, with gradient colors indicating ADE magnitude. Experiments were repeated at least two times. (b, d and e) ADE AUC quantitation for mAbs against the wildtype SARS-CoV-2 and its related point-mutant pseudoviruses (b), the Delta variant and its related point-mutant pseudoviruses (d), and the Omicron variant and its sub-lineages, as well as BA.5-R452L mutant (e).



Supplementary Fig. S6: Serological neutralization potency against SARS-CoV-2 variants.

(a) Comparative neutralizing titers (NT₅₀) of donors' sera across SARS-CoV-2 variants. Each dot represents a serum sample (n = 46). Data are presented as mean ± SD of two technical replicates. Fold change relative to wildtype for each variant shown above the line; mean value displayed below the line. Statistical analysis calculated by Kruskal-Wallis with Dunnnett's multiple comparisons and corrected with Benjamini-Hochberg adjustment. ns, not statistically significant.



Supplementary Fig. S7: Correlation analyses between volunteers' characteristics and serological ADE AUC.

(a-c) Characterization of donors' sera. Heatmap depicting in vitro ADE activity against the Delta and BA.5 variants (a), the number of prior SARS-CoV-2 infections (b), and interval time from COVID-19 recovery to blood sampling (c). NA, not available.

(d-g) Correlation analyses of ADE AUC versus the number of prior SARS-CoV-2 infections (d; $n = 40$), recovering-to-sampling interval (e; $n = 34$), volunteers' age (f; $n = 46$), and volunteers' body mass index (BMI) (g; $n = 36$). Each dot represents a serum sample. Solid lines show linear regression fits. Statistics calculated using Spearman's rank correlation method.

(h) Comparative analyses of ADE AUC between male and female donors. Statistical analyses calculated using Mann-Whitney test.

Supplementary Table S1. Comprehensive mAb panel for in vitro ADE profiling.

Summary of 114 human mAbs used in ADE assays, including 35 XG mAbs, 41 XGv mAbs and 38 structurally characterized mAbs.

Supplementary Table S2. Functional characterization of anti-S mAbs.

Binding affinity (EC_{50}) and neutralization potency (IC_{50} against SARS-CoV-2 variants) for all tested mAbs.

Supplementary Table S3. Differential cytokine gene expression in vivo across SARS-CoV-2 variants.

A curated panel of 75 cytokine-related genes analyzed by scRNA-seq, with mean expression levels and differential expression statistics across cohorts, including wildtype, Delta, and Omicron infections, as well as healthy controls.

Supplementary Table S4. Demographic and clinical characteristics of serum donors

Summary of 46 SARS-CoV-2-recovered volunteers including age, gender, vaccination status, number of prior infections, and sample collection timeline relative to diagnosis.